Transformations in a Ti-24Al-15Nb Alloy: Part I. Phase Equilibria and Microstructure

K. MURALEEDHARAN, A.K. GOGIA, T.K. NANDY, D. BANERJEE, and S. LELE

A variety of heat treatments have been employed to explore phase equilibria and the development of microstructure in a Ti-24Al-15Nb alloy. These include solution treatments both above and below the β-transus, followed by controlled cooling and aging at temperatures high enough to preclude ω-phase formation. The phase fields β, β_0, $\alpha_2 + \beta_0$, $\alpha_2 + \beta_0 + O$, and $\beta_0 + O$ have been identified in the alloy, and schematic time-temperature-transformation (TTT) curves are proposed for continuous cooling transformations from the β phase. The composition of the α_2 and β_0 phases in the $\alpha_2 + \beta_0$ region and of the α_2, β_0 and O phases in the ternary phase field have been obtained by analytical electron microscopy.

I. INTRODUCTION

THE development of Ti_3Al base alloys for high-temperature applications[1,2,3] appears to have substantially preceded the recognition of the complexity of phase equilibria and transformations in the base Ti_3Al-Nb system. It has only recently been shown that the addition of Nb to the Ti_3Al composition results not only in ordering of the β phase (B2 structure, designated β_0) but also in a distortion of the hexagonal α_2 phase (Ti_3Al, $D0_{19}$) to an orthorhombic symmetry (O, Cmcm).[4] Various other stable or metastable phases such as ω and an ω-like phase ($B8_2$ structure)[5,6,7] have also been identified, and a rigorous evaluation of high-temperature stability in the Ti-Al-Nb system is in progress.[8,9] Studies on phase equilibria and transformations in alloys along the Ti_3Al-Nb section, with Nb replacing Ti up to 25 at. pct, have also been carried out,[10–14] but the most detailed work thus far appears to be in the Ti-24Al-11Nb (24-11) composition[14,15] whose microstructure is dominated by the α_2 and β_0 phases. The O phase appears in significant amounts at Nb levels exceeding 12 at. pct[4] for Al contents of 24 to 25 pct. We have therefore chosen the Ti-24Al-15Nb (24-15) composition for a detailed study of phase transformations involving the O phase, keeping in mind that at least three alloy compositions developed thus far contain a total of β stabilizing additions up to or greater than the 15 at. pct level.[2,3,16]

II. EXPERIMENTAL

Titanium-24 at. pct Al-15 at. pct Nb was melted by consumable double-vacuum arc remelting and hot rolled below the β-transus into 12-mm-diameter bars. Table I shows the chemical composition of the alloy. The starting material for all of the heat treatments discussed in this article was the hot-rolled bar in a mill-annealed condition (slow furnace cool from 1333 K) whose microstructure is shown in Figure 1. The β-transus of the alloy, the temperature above which the alloy goes to single-phase β, was determined as 1383 ± 10 K.

The heat treatments are divided into three categories. The first (Table II) consisted of solution treatment at temperatures ranging from 1173 to 1473 K followed by water quenching. These were carried out essentially to determine the phases present at various temperatures and their volume fractions (for reasonable solution-treatment times). The second set of heat treatments (Table III) consisted of solution treatment in the single-phase β field followed by cooling at different rates to a variety of temperatures (including room temperature) followed by a water quench. These are useful in assessing the microstructures both for β heat treatment as well as for welded structures in titanium alloys. The third set of heat treatments (Table IV) consisted of aging at various temperatures ranging from 923 to 1123 K, samples which had been solution treated either above or below the β-transus. Such an aging treatment is normally required in order to stabilize the microstructure for a given high-service temperature. The aging temperatures used in this study were high enough such that isothermal β decomposition to ω or ω-related phases has not been examined. Taken together, the set of heat treatments constitute a comprehensive investigation into the variety of microstructures that may be developed in this class of alloys. Heat treatments were done in evacuated quartz capsules, back filled with argon gas in cases of section sizes less than 5 mm or in air with a protective coating when the section size was larger than 5 mm.

Thin foils for transmission electron microscopy (TEM) were made by twin-jet electropolishing in a solution containing 6 pct sulfuric acid in methanol[17] at 223 K. Transmission electron microscopy observations were made in a PHILIPS* EM 430T analytical electron microscope operating at 300 KV or in a PHILIPS CM12 analytical electron microscope operating at 120 KV, both attached with energy-dispersive spectroscopy (EDS) detectors. Fully quantitative microanalysis of individual phases was carried by analytical electron microscopy using techniques described in detail elsewhere.[18]

*PHILIPS is a trademark of Philips Electronic Instruments Corporation, Mahwah, NJ.

K. MURALEEDHARAN, Scientist, A.K. GOGIA, Scientist, T.K. NANDY, Scientist, and D. BANERJEE, Associate Director, are with the Defence Metallurgical Research Laboratory (DMRL), Hyderabad 500258, India. S. LELE, Professor, is with the Department of Metallurgical Engineering, Institute of Technology, Banaras Hindu University, Varanasi 221005, India.

Manuscript submitted June 12, 1991.

Table I. Chemical Composition of the Alloy

Element	Ti	Al	Nb	O (ppm)	N (ppm)	H (ppm)
By weight percent	bal.	13.25	29.0	810	90	18
By atomic percent	60	24.5	15.5	—	—	—

III. RESULTS

A. *Quenching Experiments*

Figures 2 through 6 show microstructures obtained after heat treatments indicated in Table II. Water quenching from above 1383 K results in retention of the β phase, but in alloys quenched from above 1403 K, fine thermal antiphase boundaries are observed (Figure 2(a)), indicating that such samples have ordered during the quench. At all solution-treatment temperatures, the β_0 phase contains a {110} tweed with ⟨110⟩ diffuse streaking (Figures 2(b) and (3)) as well as ⟨112⟩ diffuse streaking (Figure 2(c)). The intensity of the tweed appears to increase with decreasing solution-treatment temperature, as deduced from the increase in the intensity of ⟨110⟩ streaking (Figure 3).

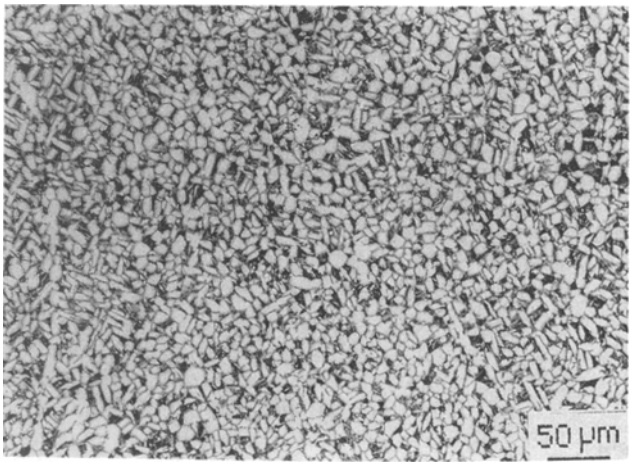

Fig. 1—Microstructure of the alloy in the MA condition, 1333 K/4 h/FCII (0.1 K/s).

Table II. Solution Treatments

Temperature (K)	Time (h)	Cooling
1473	0.5	WQ*
1423	0.5	WQ
1413	0.5	WQ
1403	0.5	WQ
1393	0.5	WQ
1383	1.0	WQ
1373	2.0	WQ
1333	4.0	WQ
1293	6.0	WQ
1253	8.0	WQ
1213	12.0	WQ
1173	16.0	WQ

*WQ = water quench.

Samples solution treated in the temperature range from 1253 to 1373 K show equiaxed α_2 grains in a β_0 matrix in optical or scanning electron micrographs (Figure 4(a)). Transmission electron microscopy (Figure 4(b)) reveals plates of the O phase at α_2/β_0 interfaces. These have been discussed in detail earlier and are believed to be a thin-foil artifact.[19] The α_2 phase shows a tweed contrast as well (Figure 5) which gives rise to barely detectable ⟨10$\bar{1}$0⟩ streaking, as seen in the [0001] zone axis.

A three-phase structure consisting of equiaxed α_2, β_0, and a coarse blocky O phase (Figure 6) is observed in samples solution treated below 1253 K. The volume fraction of the β_0 phase plotted as a function of solution-treatment temperature is shown in Figure 7 compared

Table III. β Heat Treatment: Cooling Rates and Holdings Followed by 1423 K/0.5 Hours

Cooling	Cooling Rate (K/s)	Intermediate Temperature (K)	Holding Time (h)	Final Cooling
AC	10.0	RT*	—	—
AQ	4.0	RT	—	—
FCI	0.7	RT	—	—
FCII	0.1	RT	—	—
FCIII	0.02	RT	—	—
FCII	0.1	1333	4	WQ
		1293	6	WQ
		1273	7	WQ
		1253	8	WQ
		1173	16	WQ

*RT = room temperature.

Table IV. Aging Treatments

Prior Heat Treatment	Aging Temperature (K)	Time (h)	Cooling
1293 K/6 h/WQ	1123	24	WQ
	1073	24	WQ
	1023	24	WQ
1333 K/4 h/FCII (MA)	1073	360	WQ
	923	720	WQ
β AQ	1023	24	WQ
β AQ + 1023 (24 h)	+ 923	450	WQ
β WQ	1333	4	WQ
	1273	5.5	WQ
	1213	14	WQ
	1173	40	WQ
	1073	42	WQ

*MA = mill anneal; AQ = argon quench (4 K/s); FCII = furnace cool (0.1 K/s); and WQ = water quench.

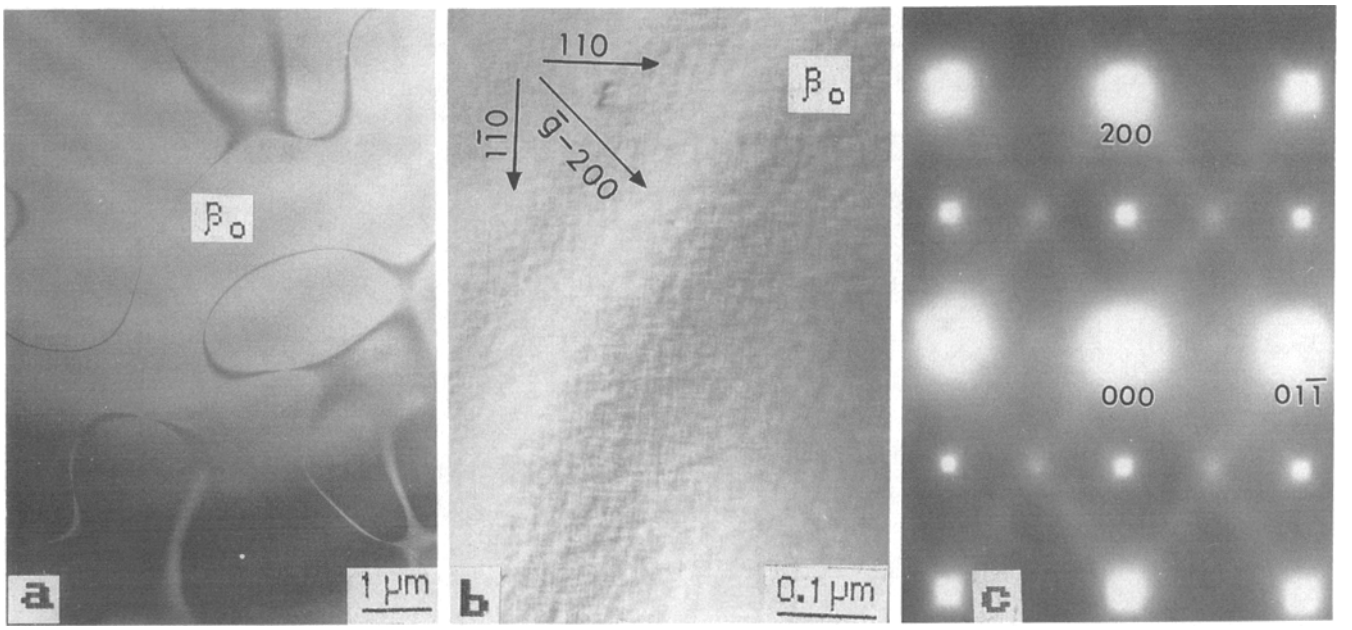

Fig. 2—Effect of water quenching from the single-phase β phase field above 1403 K. (*a*) Thermal APBs indicating $\beta \rightarrow \beta_0$ ordering during quench in specimen quenched from 1423 K, (*b*) {110} tweed, and (*c*) streaking in ⟨112⟩ directions in $[110]_{\beta_0}$ selected area diffraction pattern.

with similar data in the 24-11 alloy.[20] In the 24-15 alloy, the volume fraction of the β_0 phase is seen to be higher at all temperatures until the start of the three-phase region at 1253 K, where an abrupt decrease of the β_0 volume fraction to the levels of the 24-11 composition is observed.

Figure 8 shows the results of microanalysis on the α_2, β_0, and O phases as a function of solution-treatment temperature. The results are again compared to data generated earlier for 24-11 alloy.[18]

The difference in the α_2 and β_0 compositions between the two alloys lies essentially in the Nb content, which is higher in both the α_2 and β_0 phases of the 24-15 alloy. The O phase is seen to have a Nb content intermediate to that in the α_2 and β_0 phases, while its Al content is similar to that of the α_2 phase.

B. *The Effect of Cooling Rate on β Solution-Treated Structures*

We first show microstructures (Figure 9) obtained by furnace cooling to different temperatures followed by a hold and quench (Table III). The difference between this set of heat treatments and that of the previous set lies in the starting structure which was essentially α_2 in the previous case (Figure 1) and is the β phase (obtained by β solution treatment) in this set. However, the phases seen are identical, although the microstructures are different. Cooling to temperatures as low as 1273 K results in only the α_2 phase precipitated in a Burgers orientation to β_0 (Figure 9(a)). Interestingly, no O phase is observed at the α_2/β_0 interfaces after this heat treatment, in contrast to Figure 4, in agreement with the suggestion that it may

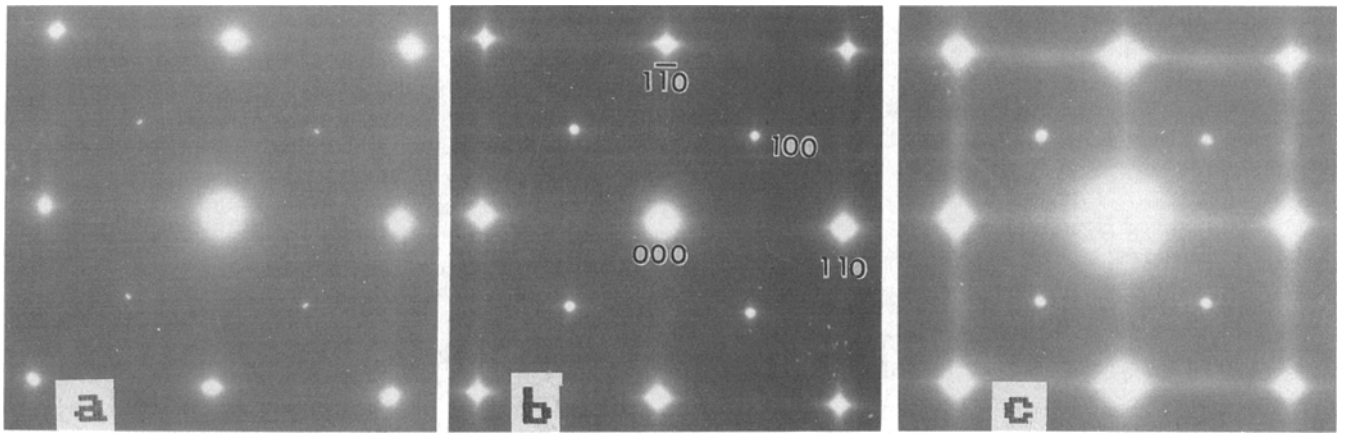

Fig. 3—Intensification of the ⟨110⟩ diffused streaking in [001] diffraction patterns from samples at (*a*) 1473 K, (*b*) 1423 K, and (*c*) 1333 K.

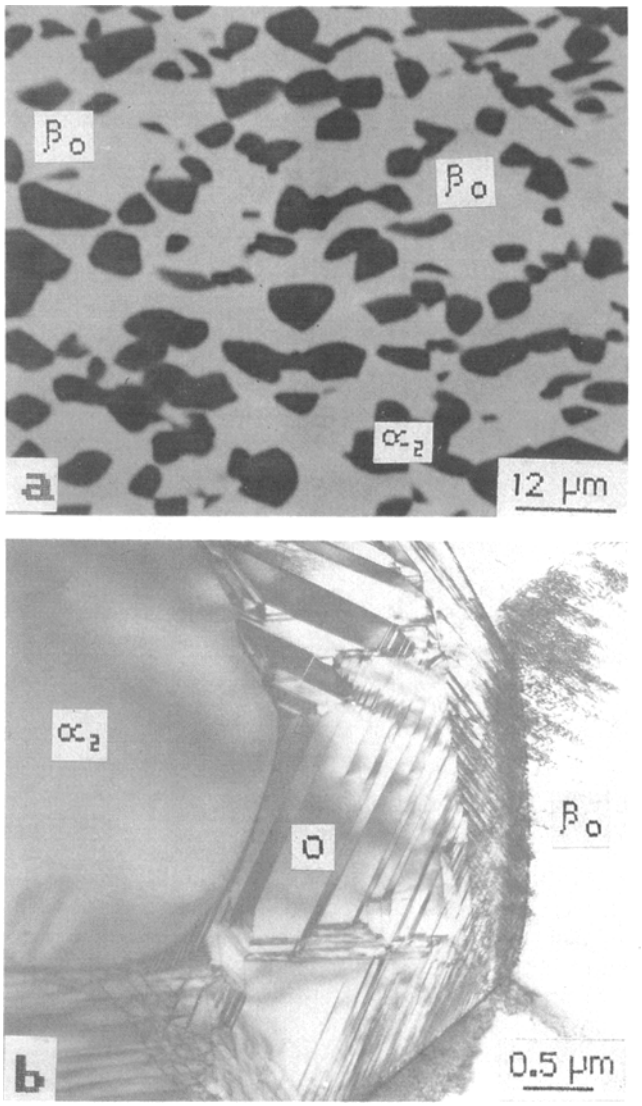

Fig. 4—Microstructure in the alloy solution-treated at 1293 K: (*a*) scanning electron microscopy (SEM) back-scattered electron micrograph showing α_2 and β_0 phases and (*b*) TEM BF showing the O phase at α_2/β_0 interfaces.

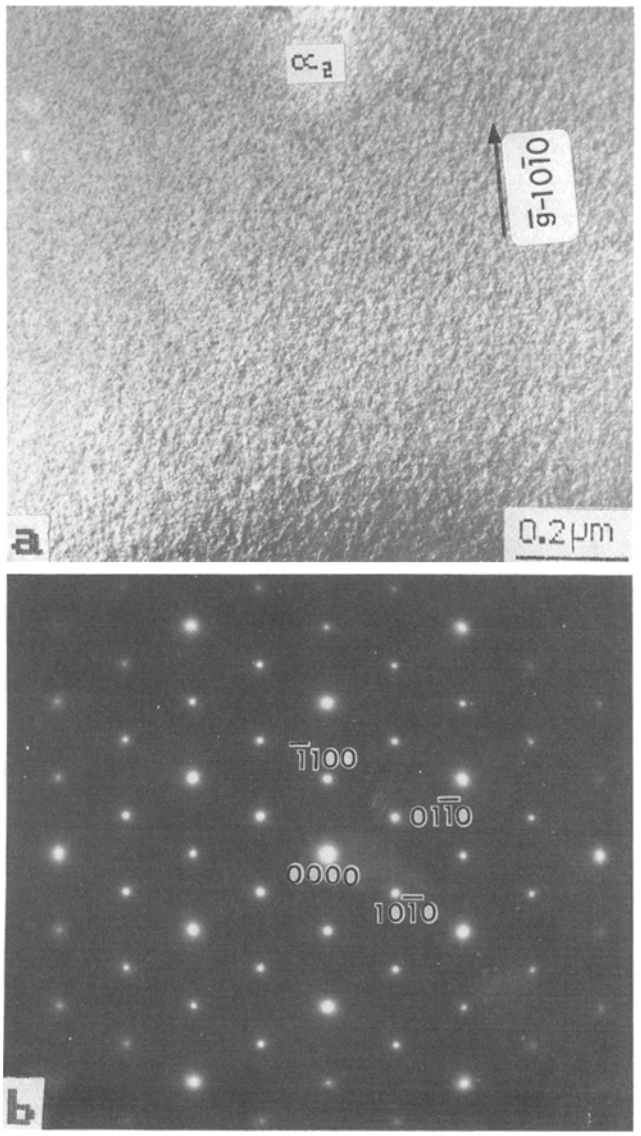

Fig. 5—Tweed contrast observed within the α_2 phase. (*a*) Tweed contrast imaged with $10\bar{1}0_{\alpha_2}$ reflection. (*b*) Diffuse streaking in $\langle 10\bar{1}0\rangle$ directions in [0001] zone axis. Specimen heat-treated at 1333 K/4 h/WQ.

be an artifact of thin-foil preparation for the specific heat treatment. In samples cooled to 1253 K, a platelike O phase precipitates at the periphery of the α_2 phase (Figure 9(b)), while samples cooled to 1173 K show, in addition, a large amount of monolithic O phase enveloping the α_2 + O structure (Figure 9(c)).

The microstructure of samples cooled at different rates to room temperature are shown in Figures 10 and 11. At the cooling rate of 10 K/s (air cool), occasional large patches of retained β_0 are present which contain thermal antiphase boundaries (APBs) and the tweed microstructure. The major portions of the structure contain relatively large O plates, between which there is a finer distribution of O plates (Figure 10(a)). At slower cooling rates of 4 and 0.7 K/s, the patches of retained β_0 are completely absent, and a structure of O laths with films of retained β_0 is seen (Figures 10(b) and (c)). At still slower cooling rates, the lath microstructure is considerably more complex. Three types of lath structure are observed at this cooling rate—the first consists of O laths and retained β_0 as in faster cooled structures (Figure 11(a)), the second consists of laths with a core of fine, multivariant O plates surrounded by monolithic O (Figure 11(b)), and the third consists of laths with a core of α_2 phase surrounded by plate O and then a layer of monolithic O (Figure 11(c)). It is noted that foil sectioning effects can produce these three structure types from a lath structure which is basically of the third kind. The various phases have been identified through diffraction, as shown in Figure 12.

C. *Aged Structures*

1. *Aging α_2 + β_0 structures*

Specimens chosen for aging treatments were solution treated at 1293 K in the α_2 + β_0 region, followed by

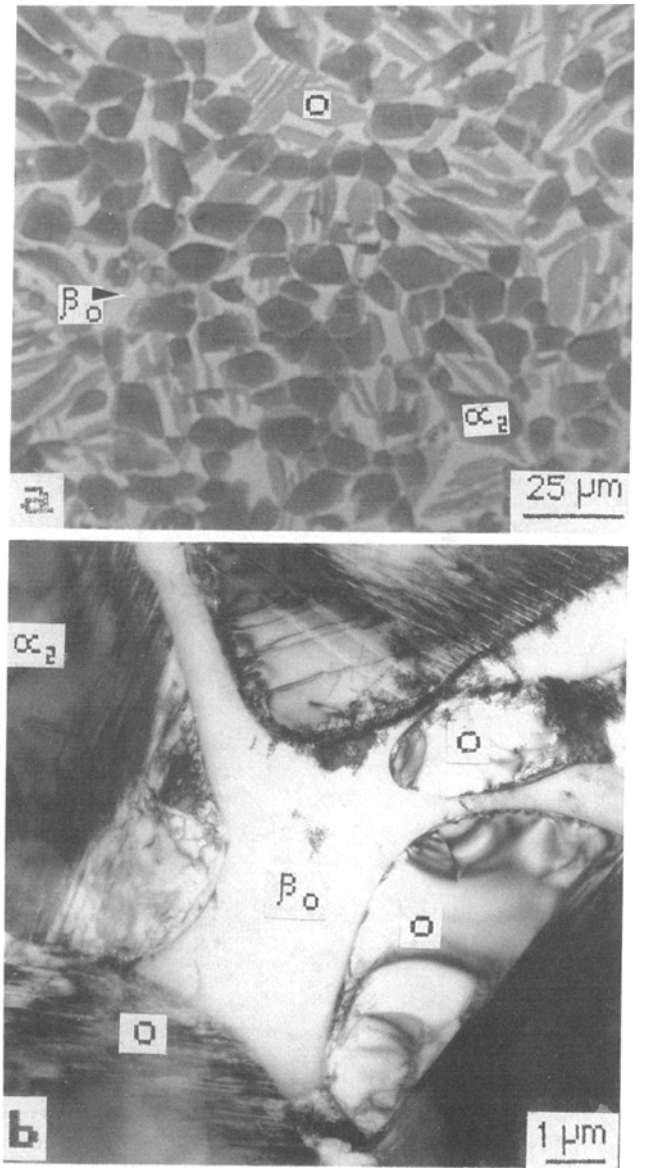

Fig. 6—Three-phase structure observed in the alloy solution treated at 1173 K. (*a*) SEM back-scattered micrograph, showing α_2, O, and β_0 phases. The O phase shows a gray contrast, indicating its Nb content to lie between those of the α_2 and β_0 phases. (*b*) BF TEM micrographs showing blocky O phase.

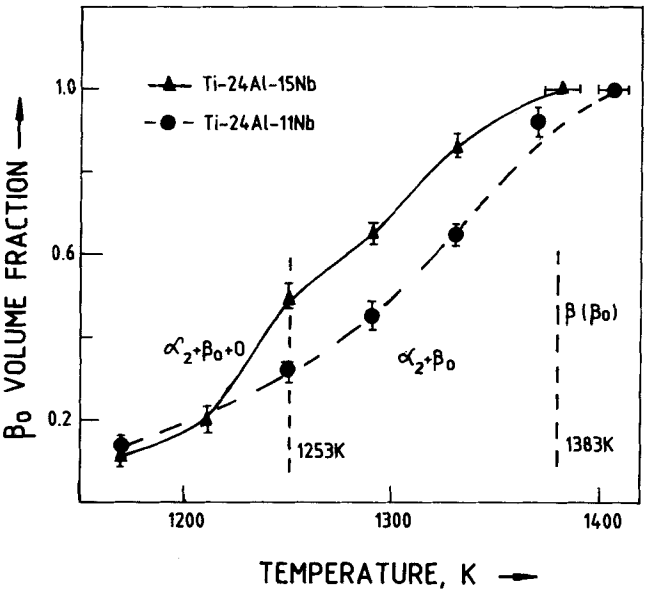

Fig. 7—Volume fraction of β_0 phase plotted as a function of solution-treatment temperature. Dotted lines indicate data on Ti-24Al-11Nb alloy.[20]

water quenching. The microstructure prior to aging consists of equiaxed α_2 particles in a β_0 matrix. We consider in the following paragraphs transformations occurring both within primary α_2 phase ($P\alpha_2$), the β_0 matrix phase, and the $P\alpha_2/\beta_0$ interface. Aging done at temperatures from 1023 to 1123 K all resulted in identical microstructures.

A monolithic O phase develops at the periphery of the $P\alpha_2$ phase (Figure 13(a)). Just next to this periphery, within the $P\alpha_2$ phase, there is a region made up of fine O plates, as shown in Figure 13(b). It is also observed that the interior of the $P\alpha_2$ phase is marked by a strong mottling.

The aged β_0 contains two distinctly different transformation products within the same specimen at all aging temperatures 1023 to 1123 K. In the first case, as shown in Figure 14(a), the β_0 phase has transformed to O, within which fine β_0 plates are observed. Almost all of the prior β_0 grain has thus transformed to O of the same orientation. In the second type of transformation, different variants of O phase are nucleated in a continuous manner, with β_0 retained as a thin film between O plates, as shown in the TEM bright-field (BF) image in Figure 14(b). The selected area diffraction pattern (SADP) in Figure 14(c) shows the diffraction pattern from the three variants of O phase along with the parent β_0 phase in a $[111]_{\beta_0}$ orientation. The orientation relationship between O and β_0 phase is $(001)_O//(110)_{\beta_0}$ and $[110]_O//[1\bar{1}1]_{\beta_0}$. Thus, in a $[1\bar{1}1]_{\beta_0}$ orientation, three variants of

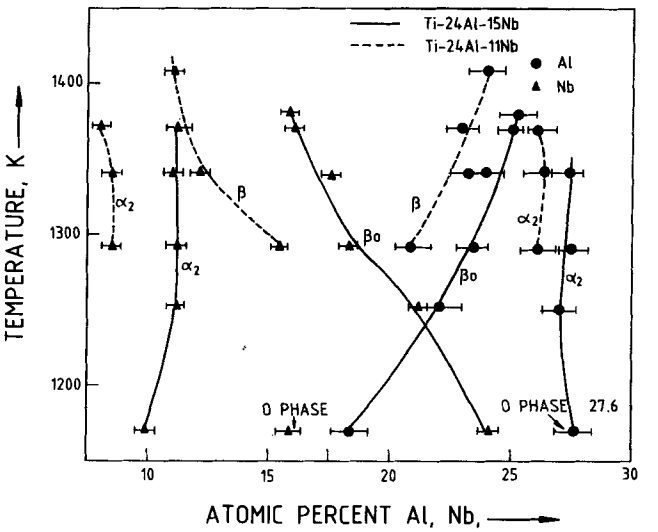

Fig. 8—Chemical composition of α_2 and β_0 phases in atomic percent plotted as a function of solution-treatment temperature. Dotted lines indicate data from Ti-24Al-11Nb alloy.[18] Al and Nb concentrations of O phase at 1173 K are also indicated.

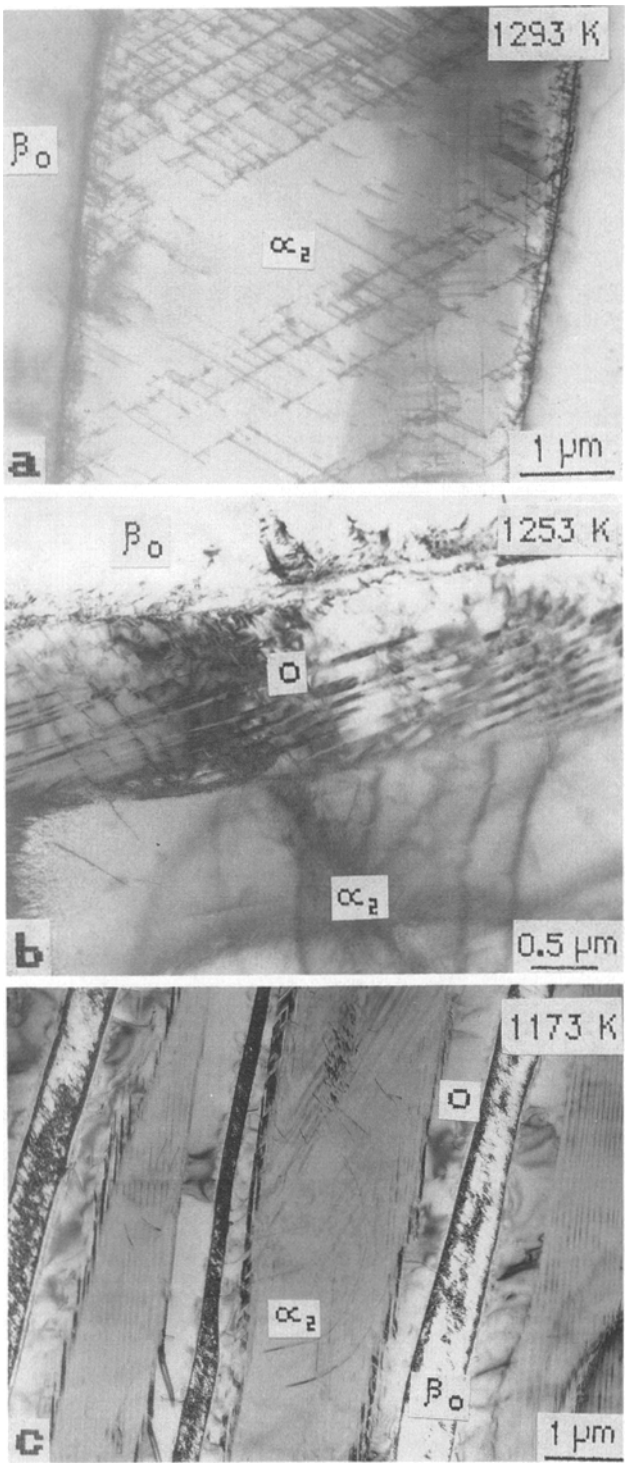

Fig. 9—Microstructures obtained by furnace cooling to intermediate temperatures from β followed by hold and water quenching. TEM BF micrographs after holding at (*a*) 1293 K, (*b*) 1253 K, and (*c*) 1173 K, respectively.

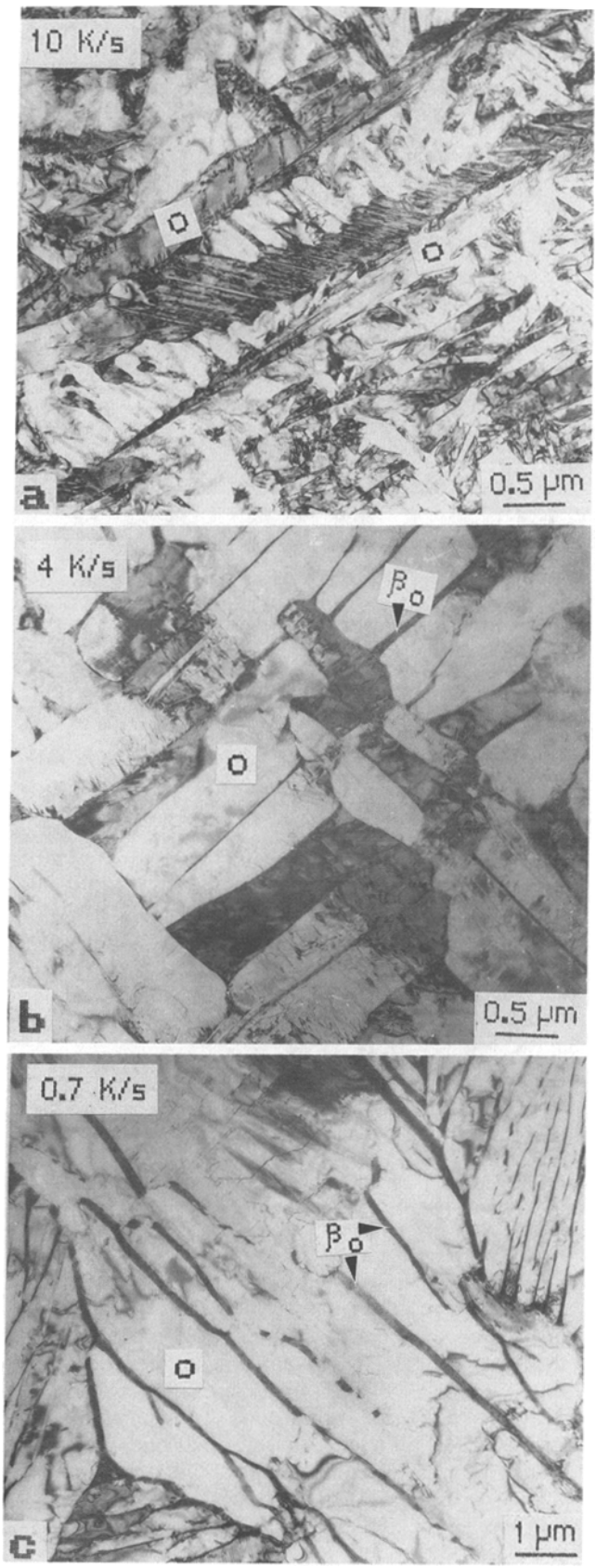

Fig. 10—Microstructures in specimens cooled to room temperature from β: (*a*) TEM BF showing coarse and fine O laths in sample cooled at 10 K/s, (*b*) O + β_0 structures obtained in specimens cooled at 4 K/s from β, and (*c*) O + β_0 structure in specimens cooled at 0.7 K/s.

the O phase are seen, with $(001)_O$ parallel to each of the three $\{110\}_{\beta_0}$ planes. All of the O variants share a common $[110]_O$ direction with $[111]_{\beta_0}$.

Quantitative microanalysis using EDS was also performed on one of the specimens aged at 1073 K for 24 hours, and the results are shown in Table V. The Pα_2

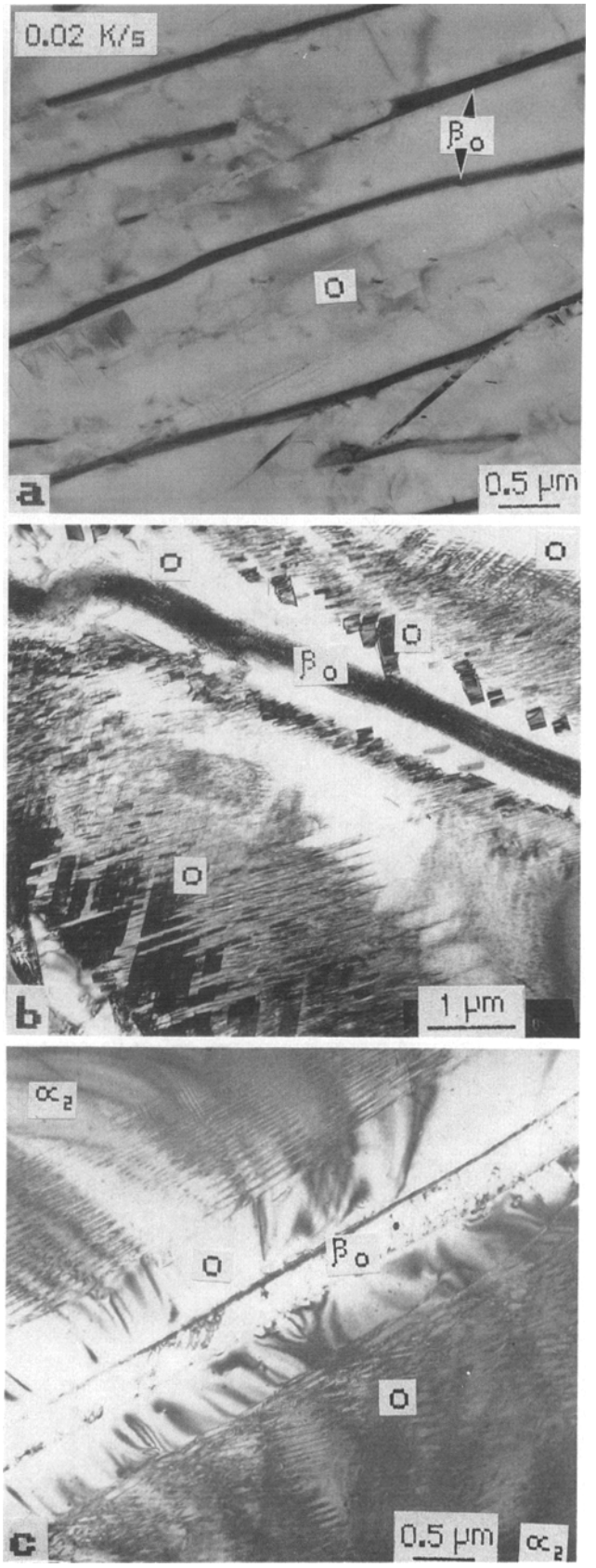

Fig. 11—Lath structures obtained in specimens slow furnace cooled from β at 0.02 K/s: (*a*) O + β_0 structure, (*b*) O laths with multivariant plate O in the core and monolithic O at periphery, and (*c*) laths with α_2 in the core and plate O and monolithic O.

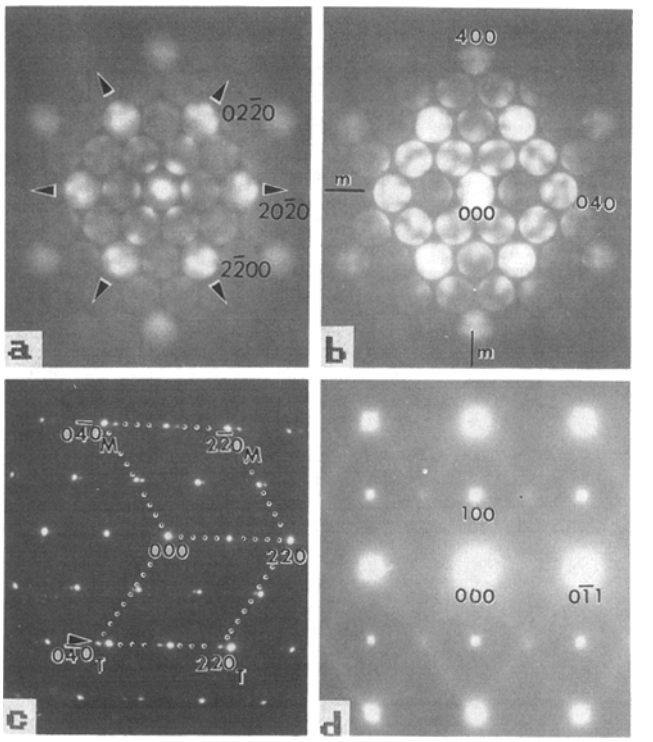

Fig. 12—Diffraction patterns obtained from various phases: (*a*) α_2, [0001] zone axis, (*b*) monolithic O, [001] zone axis, (*c*) plate O, twin-related variants both in the [001] zone axis, and (*d*) β_0, [011] zone axis.

phase has a chemistry similar to that of α_2 phase in the specimen quenched from 1073 K. The twin related plate-like O phase found at the periphery of the primary α_2 plates (Figure 13) yielded compositions of 15.7 at. pct Nb, while the monolithic O around primary α_2 (Figure 13) contained 20.1 pct Nb. Aluminum compositions of both the twinned O and monolithic O were in the range of 26.1 to 27.6 Al. Also shown are the chemical analyses of the O and β_0 phases in the aged β_0. The O phase produced from the first type of aging transformation has a chemical composition of 26.5 at. pct Al and 15.4 at. pct Nb, which is close to the composition of the 24-15 alloy. The decomposition product of the continuous transformation, the O plates, and β_0 particles were very fine and, hence, did not allow very accurate composition determination. Nevertheless, the results obtained are indicated in Table V.

The effect of aging at a still lower temperature (923 K) for 720 hours on primary α_2 phase is shown in Figure 15. The microstructure chosen for aging at this temperature was not the α_2 + β_0 structure quenched from 1293 K but the mill-annealed structure shown in Figure 1. This structure was slow furnace cooled (0.1 K/s) to room temperature after homogenization at 1333 K and, therefore, was expected to be closer to the equilibrium in terms of volume fraction and chemical compositions for various phases at 923 K. The objective was to see if the primary α_2 phase would transform to O, since as described in Section III–C–3, there was reason to believe that a two-phase O + β_0 region exists at these temperatures. Figure 15(a) is a BF TEM

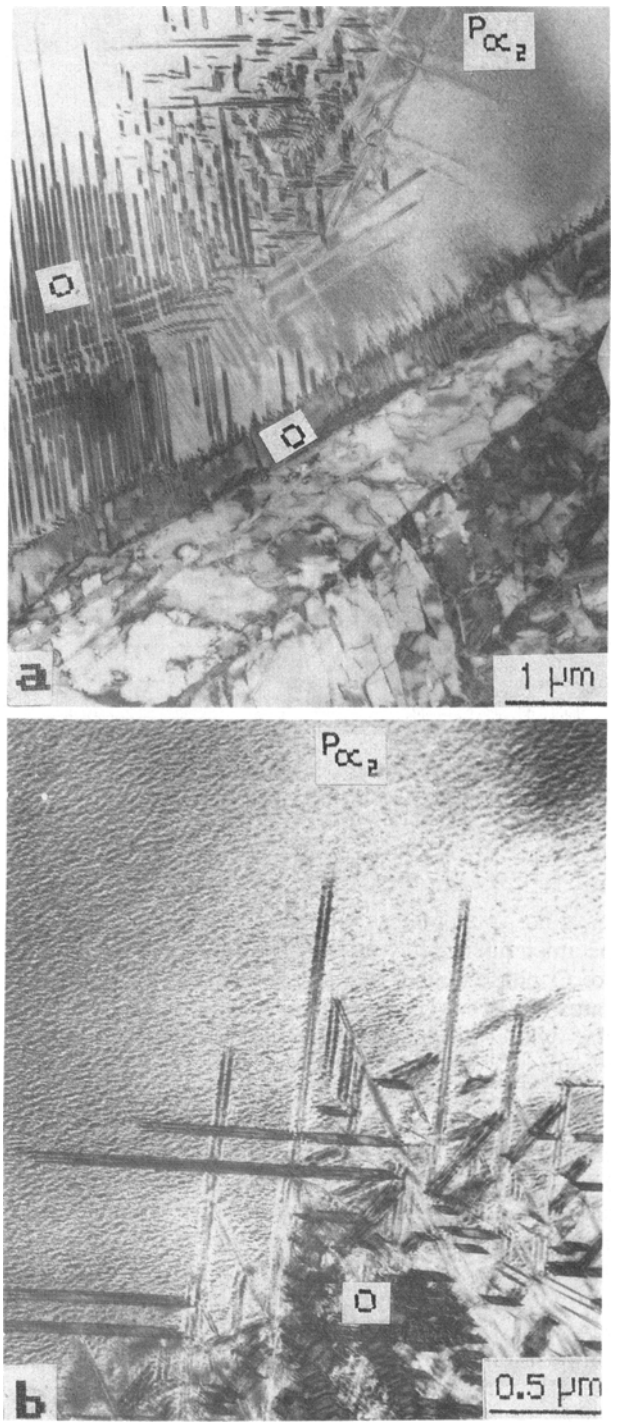

Fig. 13—Effect of aging on transformations within primary α_2 and at the α_2/β_0 interface for aging temperatures ranging from 1023 to 1123 K: (*a*) formation of monolithic O at the interface and (*b*) precipitation of O plates within primary α_2 and enhanced tweed within primary α_2 in a specimen aged at 1073 K/24 h/WQ.

micrograph showing a primary α_2 particle which has the platelike O periphery and the interior of which shows an enhanced tweed contrast (compare with Figure 5). This tweed can now be assigned definite crystallographic directions. Figure 15(b) shows the tweed with two intensity modulations at approximately 60 deg to each other imaged with a $22\bar{4}0$ type of α_2 reflection close to the

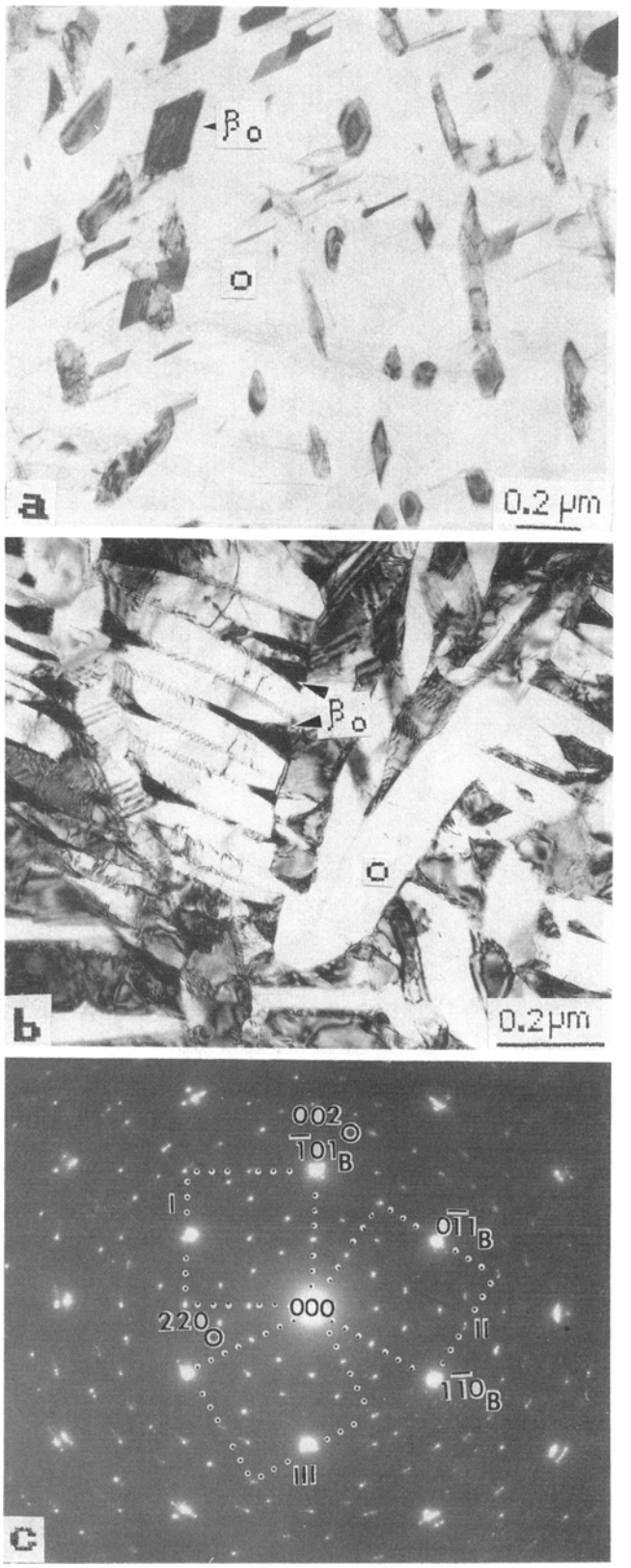

Fig. 14—(*a*) Massive O with β_0 precipitates after aging at 1023 K, (*b*) discontinuous precipitation of O in β_0 in the same specimen at different area, and (*c*) SAD from the region showing three variants of O phase in ⟨110⟩ zone axes with $[111]_{\beta_0}$ zone axis. The microstructures observed at aging temperatures of 1073 and 1123 K were similar.

Table V. Results of Microanalysis on Specimen Aged at 1073 K

Phase	Microstructural Details	Chemical Composition (At. Pct)		
		Ti	Al	Nb
$P\alpha_2$	within $P\alpha_2$	61.5 ± 0.4	27.2 ± 0.6	11.3 ± 0.3
O	plate O periphery	56.7 ± 0.3	27.6 ± 0.5	15.7 ± 0.2
	peritectoid O	53.7 ± 0.3	26.2 ± 0.6	20.1 ± 0.1
Aged β_0	O (discontinuous)	58.1 ± 0.3	26.1 ± 0.8	15.8 ± 0.1
	O (massive)	58.1 ± 0.4	26.5 ± 0.5	15.4 ± 0.3
	retained β_0	52.1 ± 0.5	22.4 ± 0.7	25.5 ± 0.2

basal zone axis. As in Figure 5, there is evidence of diffuse streaking in the $[0001]_{\alpha_2}$ diffraction patterns along the three $\langle 10\bar{1}0\rangle$ directions. However, under the imaging conditions in Figure 15(b), the striations in the tweed are seen to be nearly parallel to the two $\{10\bar{1}0\}$ planes 30 deg on either side of the imaging $22\bar{4}0$, while striations parallel to that $\{10\bar{1}0\}$ plane perpendicular to the imaging reflection are not observed. At a higher aging temperature of 1073 K, the mill-annealed (MA) structure did not show such effects, even after aging for 360 hours.

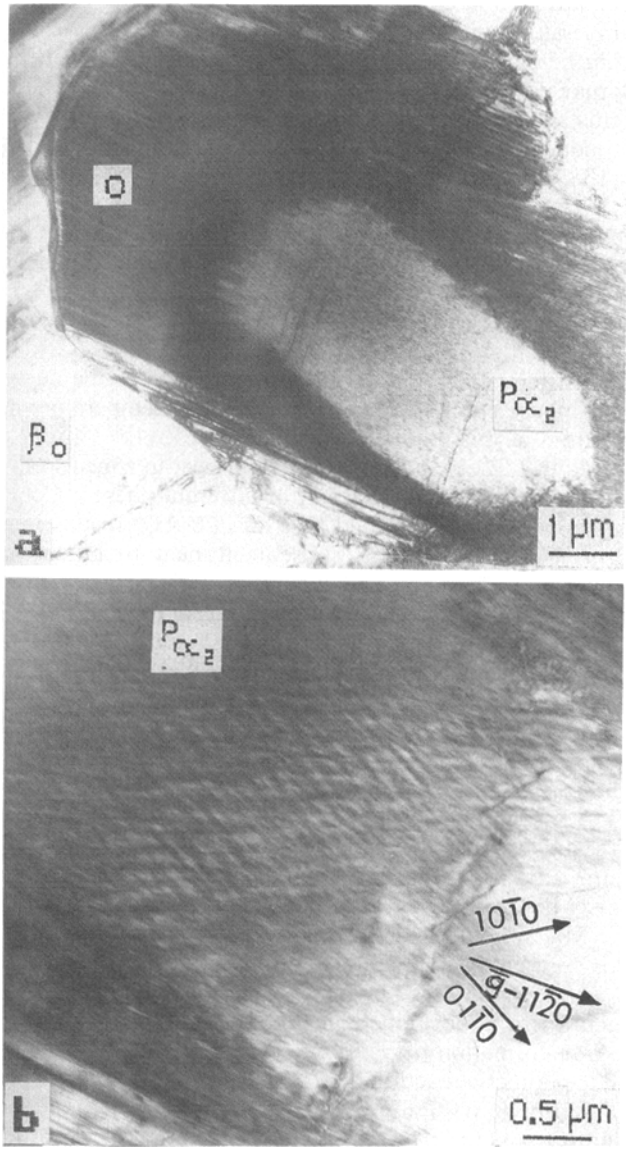

Fig. 15—Effect of aging at 923 K for 720 h on the MA structure: (*a*) BF of α_2 particle and (*b*) $\{10\bar{1}0\}$ tweed in two directions at 60 deg to each other.

2. *Aging β argon-quenched (AQ) structures*

Aging of the β AQ specimens was carried out in the temperature range from 923 to 1023 K, and the results are shown in Figure 16. Such treatments were carried out to determine whether the two-phase O + β_0 structure formed by argon quenching would decompose to a three-phase α_2 + β_0 + O structure. Aging for 24 hours at 1023 K revealed the precipitation of new grains at the O/β_0 interfaces, as shown in Figure 16(a). Selected area diffraction patterns confirmed this phase to be orthorhombic. Subsequent aging at 923 K for 450 hours resulted in the formation of more equiaxed O grains (Figure 16(b)). A comparison with Figure 10(b) shows that the microstructure consists of a large number of fine grains after such an aging treatment. No α_2 phase was detected.

3. *Aging of β water-quenched (WQ) structures*

Water quenching from the β phase field results in the retention of β_0 as a metastable phase, and the decomposition of this phase on aging at temperatures between 1073 and 1323 K is shown in Figure 17. The aging times chosen were similar to those used in the aging of subtransus solution treatments discussed earlier, and the difference is essentially in the starting composition of the parent β_0, which is that of the alloy in this case. The effect of aging for shorter durations and the sequence of β_0 phase decomposition are discussed in Part II.[21] Here, we focus our attention on the phases obtained after longer exposures.

Figure 17(a) shows a TEM BF micrograph of the specimen aged at 1273 K for 5.5 hours followed by water quenching. It contains α_2 plates and β_0 in the Burgers' relationship. The α_2, O, and β_0 phases are formed on aging at 1213 K for 14 hours, and the microstructure is shown in Figure 17(b). The microstructure consists of alternate α_2 and O plates within broad bands. Also seen are β_0 precipitates within the broad bands. At still lower aging temperatures (1173 K), α_2, O, and β_0 phases were again present but with considerably lower volume fractions of α_2. The α_2 phase is present as very thin plates within O laths, as shown in Figure 17(c). The β_0 phase is present as relatively coarser precipitates. Aging at 1073 K for 42 hours resulted in a O + β_0 microstructure.

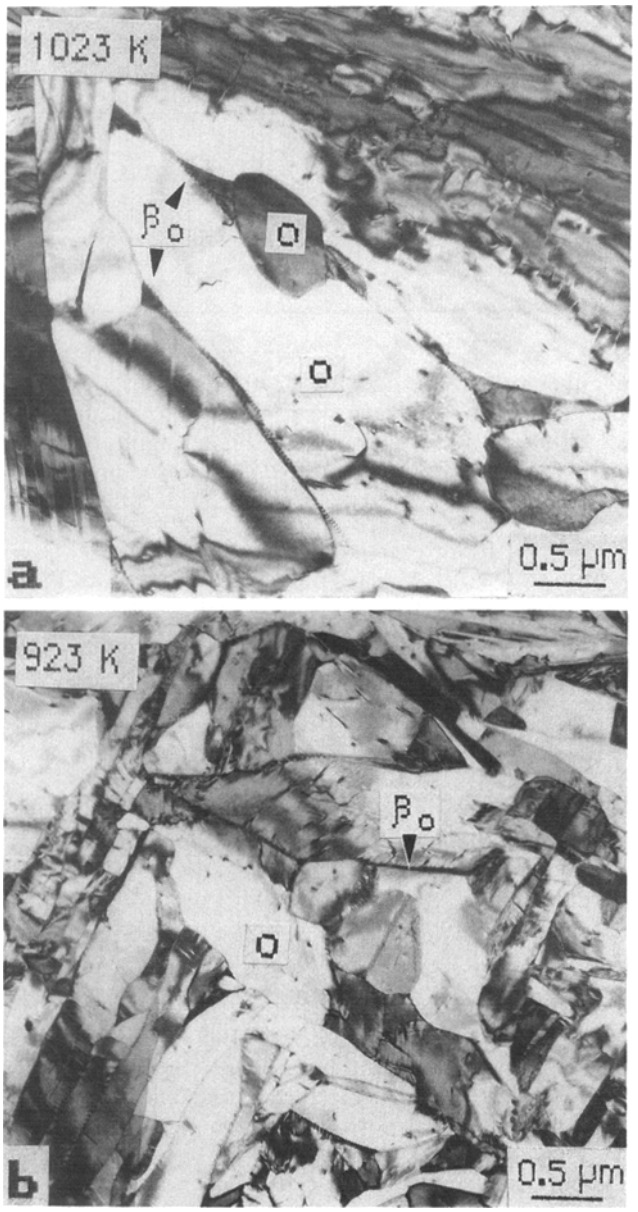

Fig. 16—Recrystallization of O + β_0 microstructure during aging: (*a*) after 24 h at 1023 K (see precipitation of fresh O grains as marked) and (*b*) after subsequent aging at 923 K for 450 h [compare the recrystallized structure consisting of finer grains with the starting microstructure of β AQ (Fig. 10(b))].

The β_0 phase was present as fine precipitates in a matrix of O, and the microstructure is shown in Figure 17(d). The identification of phases was carried out by analysis of SAD patterns, as shown in Figure 18.

IV. DISCUSSION

A. *Phase Equilibria*

Subsequent to the identification of the orthorhombic phase,[4] we proposed[10] the schematic phase diagram shown in Figure 19 for the Ti_3-Al-Nb section. This vertical section was developed from the reactions expected to occur given the existence of the β, β_0, α, α_2, and O phases. The results presented in this article appear to constitute the first experimental evidence that some of the phase fields shown in Figure 19 do indeed exist. A summary of the phase field shown in Figure 19 do indeed exist. A summary of the various phases observed as a result of heat treatments at different temperatures for the 24-15 alloy is given in Figure 20. The figure lists the final heat-treatment temperature prior to water quenching as well as the different thermal paths adopted to reach the final temperature. Rather than follow conventional methods of heat treatment at increasingly long times with decreasing temperature to obtain the equilibrium phases, we have consciously adopted a different approach, that of employing alternative kinetic routes toward equilibrium and then looking for agreement in the phases observed at the same final temperature.

The order-disorder temperature for the β phase ($\beta \rightarrow$ B2) is 1403 K based upon the observation of thermal antiphase domains in samples quenched from above this temperature and the lack of them in samples quenched from below this temperature. A two-phase region β + β_0 may not exist between the single-phase β and β_0 phase fields should this be a second-order transformation. The boundary between the β_0 and α_2 + β_0 phase fields lies at 1383 K and that between the α_2 + β_0 and α_2 + O + β_0 phase fields at 1253 K with good agreement in the phases observed at the same final heat-treatment temperature after different prior heat treatments down to 1173 K. The transus between the α_2 + β_0 and α_2 + O + β_0 phase fields (1125 K) is also clearly demarcated by the discontinuities in the curve of β_0 volume fraction against temperature in Figure 7, as well as in the curve of β_0 phase composition (Nb pct) against temperature in Figure 8 at this temperature of 1253 K.

Below 1123 K, however, different heat-treatment paths to the final temperature result in different phases. Cooling from the β phase field at 4 K/s (β AQ) results in a O + β_0 structure, and subsequent heat treatment at 1023 K for 24 hours and then at 923 K for as long as 450 hours results in no additional phase formation. Direct heat treatment for as long as 42 hours at 1023 K subsequent to water quenching from the β phase also results in the formation of O and β_0 phases.

However, if the α_2 phase has been formed by a previous heat treatment such as the MA (Pα_2), then this phase is retained, even after long-term exposure below 1123 K such that all three phases α_2, O, and β_0 are seen. We suggest that the latter observation is a nonequilibrium result, and that a two-phase field O + β_0 actually exists below 1123 K. This suggestion is made because the MA structures develop a rim of O phase around the Pα_2 on aging, apparently through a reaction α_2 + $\beta_0 \rightarrow$ O, as discussed in greater detail in Section B. Once such a rim is developed, it effectively acts as a barrier to transformation of α_2 to O in analogy with the incomplete peritectic reaction.[22] The other two heat treatments (β AQ or β WQ) allow direct formation of the equilibrium O structure, thus circumventing this kinetic difficulty in transforming Pα_2 to O. Based on the current results, the (α_2 + β_0 + O)/(β_0 + O) phase boundary transus is suggested to lie between 1073 and 1173 K.

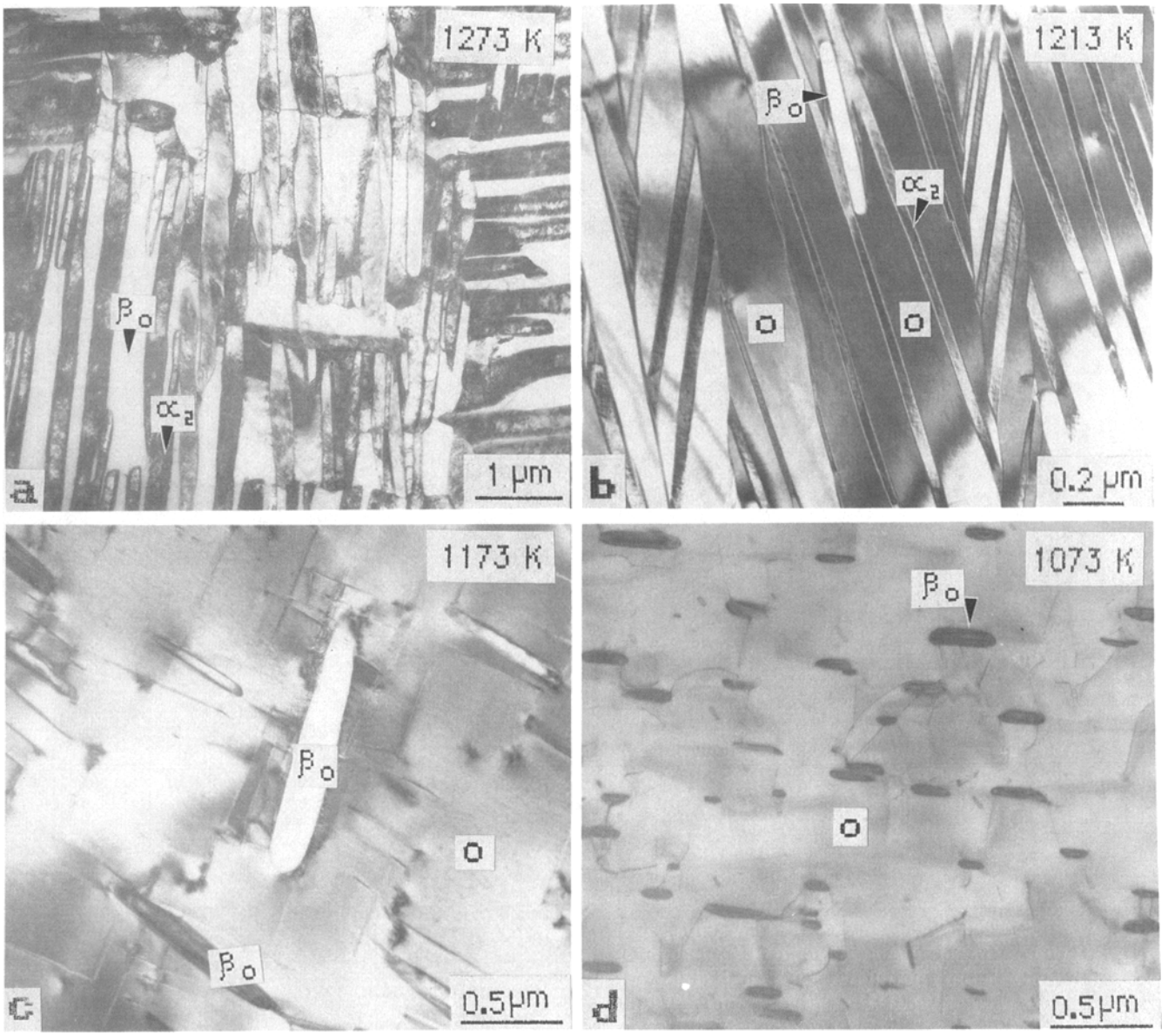

Fig. 17—BF TEM micrographs showing phases present in specimen β WQ and aged: (*a*) α_2 + β_0 phases, 1273 K; (*b*) O + α_2 + β_0 phases, 1213 K; (*c*) O + α_2 + β_0 phases, 1173 K; and (*d*) O + β_0 phases, 1073 K.

The analytical work carried out in this study allows us to define the three-phase field α_2 + β_0 + O at 1173 K, as shown in Figure 21. The corners of this phase field are connected to the relevant points of the binary sections Ti-Al and Ti-Nb at this temperature.

The compositions of the α_2 and β (β_0) phases of the 24-15 and 24-11 alloys have been given in Figure 8. Several points of interest are emphasized here. (1) The Al content of the α_2 phase lies between 26 and 27 at. pct, rather than at 25 at. pct, as might be expected for an A_3B compound. The data agree with that of Kestner-Weykamp *et al.*[13] It is felt, however, that this is consistent in terms of the binary Ti-Al diagram, where the critical α_2 order-disorder transformation temperature has been shown to peak at about 30 at. pct Al.[23] (2) While the Al content of the α_2 phase in the 24-11 and 24-15 alloys is very similar, the α_2 phase of 24-15 has a higher Nb solubility than that of 24-11. It is noted in this context that the α_2 in 24-11 is in equilibrium with disordered β,[12,15] while that in 24-15 alloy is in equilibrium with β_0 over the temperature range under discussion. (3) Both the Nb and Al levels of β_0 in 24-15 are higher than in 24-11, in which the β phase is disordered at this temperature. This must be responsible for the steep rise of the order-disorder temperature which lies above the β transus in the 24-15 alloy. (4) Finally, we note that the Al content of the β_0 phase decreases down to 18 pct in the three-phase α_2 + β_0 + O region at 1173 K. Nevertheless, the β_0 phase remains ordered, unlike in the 24-11 alloy, where disordering has been reported at 1173 K due to the decreasing Al level (again ~18 pct).[13] This is perhaps because the Nb level in 24-15

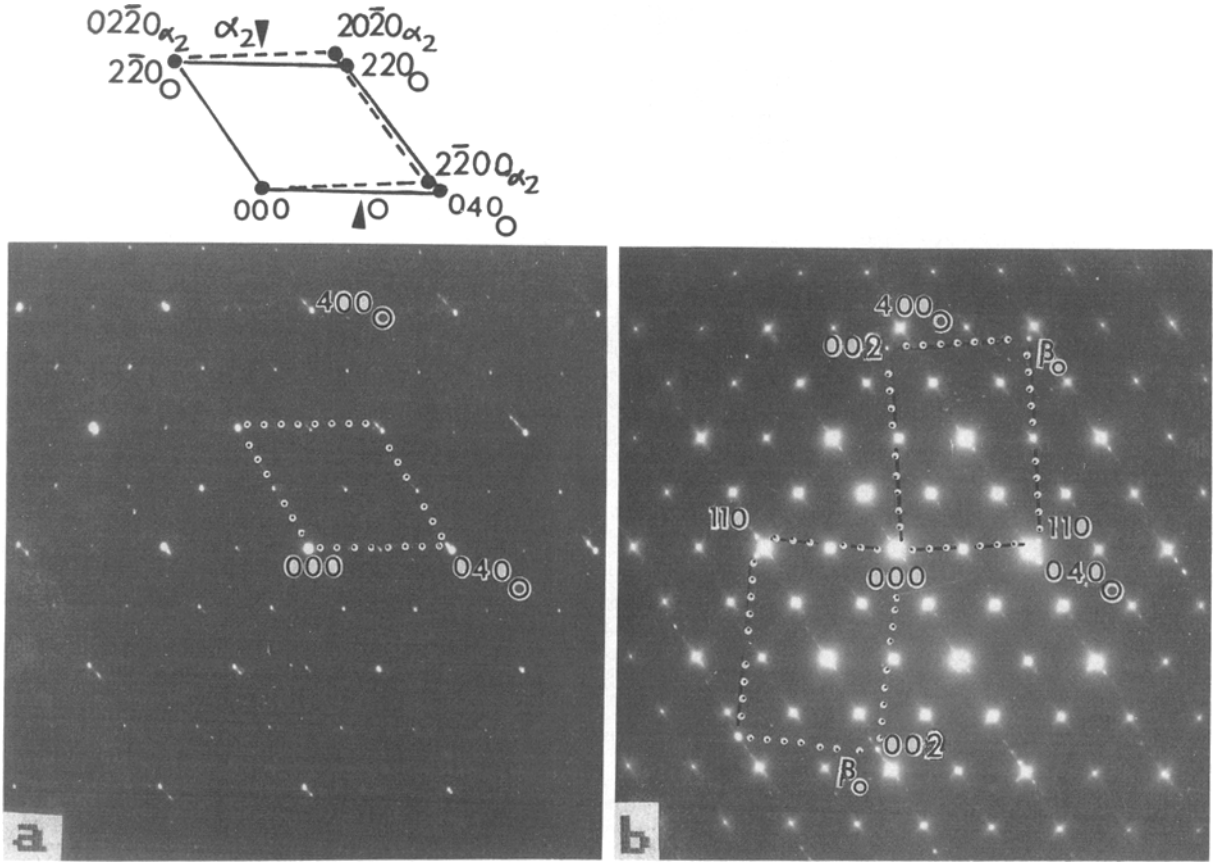

Fig. 18—SADPs of α_2, O, and β_0 phases from samples β WQ and aged, 1073 to 1273 K: (*a*) α_2 in [0001] and 0 in [001] zone axes (contrast this with Fig. 12(c), which contains two variants of the O phase) and (*b*) 0 in [001] zone axis with two β_0 variants both in ⟨110⟩ zone axes.

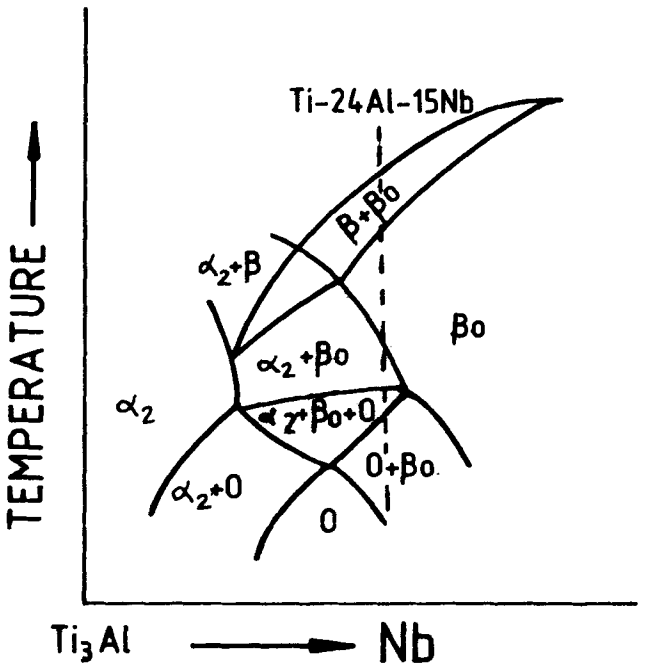

Fig. 19—A schematic phase diagram proposed for the Ti_3Al-Nb section.[10] Dotted vertical line indicates the possible location of Ti-24Al-15Nb composition on such a section.

(~24 pct) at this temperature is considerably higher than in 24-11 (~16.5 pct).

B. *Transformations on Cooling from the β Phase Field*

The results obtained from heat treatments in the single-phase β field followed by subsequent cooling at different rates allow us to postulate a set of schematic time-temperature-transformation (TTT) curves for the continuous cooling transformations. While recent attempts at defining such curves for the Ti-25Al-10Nb-3V-1Mo alloy are more quantitative in that transformation temperature and times are defined by dilatometric techniques,[24,25] it is felt that they are inadequate in that they do not distinguish between the variety of transformation paths that exist in this class of alloys.

The results of the previous section on phase equilibria (Figure 19) may be combined with the data presented on the cooling transformation to generate Figure 22. Since cooling rates ranging from 10 to 0.7 K/s result in O phase precipitation in these samples, the TTT curve for the transformation $\beta_0 \rightarrow \beta_0 + O$ is constructed to allow an intersection with the cooling curves for these cooling rates. Further, large retained β_0 patches for the β AC treatment indicate that this cooling curve just passes through the nose of the TTT curve. The curve has been

HEAT TREATMENTS AND PHASES OBSERVED IN Ti-24Al-15Nb

HEAT TREATMENT	RANGE OF FINAL HT TEMPERATURE, K	PHASES OBSERVED
MA + ST/WQ	1413 - 1473	β
MA + ST/WQ	1383 - 1403	β_o
MA + ST/WQ	1253 - 1373	$\alpha_2 + \beta_o$
$\beta \xrightarrow{FC}$ HOLD/WQ	1273 - 1333	$\alpha_2 + \beta_o$
β WQ + AGE/WQ	1273 - 1323	$\alpha_2 + \beta_o$
MA + ST/WQ	1173 - 1213	$\alpha_2 + O + \beta_o$
$\beta \xrightarrow{FC}$ HOLD/WQ	1173 - 1253	$\alpha_2 + O + \beta_o$
β WQ + AGE/WQ	1173 - 1213	$\alpha_2 + O + \beta_o$
MA + $\alpha_2 + \beta_o$ ST + AGE	1023 - 1123	$(\alpha_2) + O + \beta_o^*$
β WQ + AGE	1073	$O + \beta_o$
β AQ ($O + \beta_o$) + AGE	923 - 1023	$O + \beta_o$

* α_2 IS THE PRIMARY α_2 PHASE RESULTING FROM THE $\alpha_2 + \beta_o$ ST AND NOT TRANSFORMED
MA - MILL ANNEAL, ST - SOLUTION TREAT
WQ - WATER QUENCH, FC - FURNACE COOL, 0.1K/sec.
AQ - ARGON QUENCH, 4 K/sec.

Fig. 20—A summary of heat treatment and phases observed leading to the boundaries between various phase fields, shown on the right-hand side of the figure (see text for a discussion).

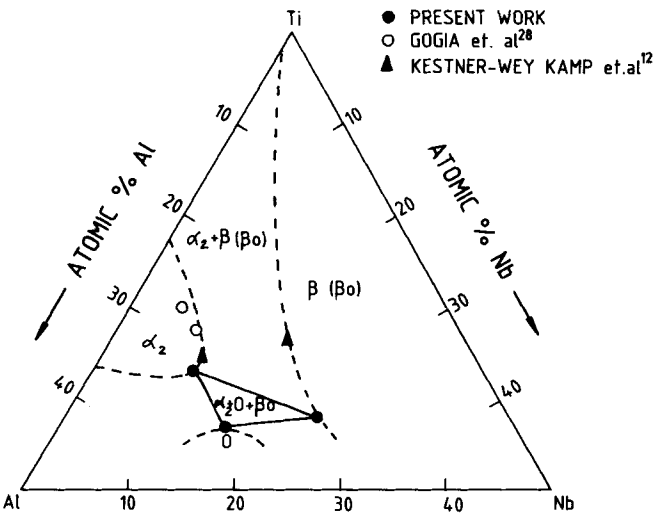

Fig. 21—The ternary $\alpha_2 + \beta_0 + O$ triangle at 1173 K. The $\alpha_2 + \beta$ and $\alpha_2 + \beta_0$ phase fields have not been shown separately for simplicity.

made asymptotic to the transus temperature between the $\alpha_2 + \beta_0$ and $\alpha_2 + \beta_0 + O$ phase fields. Strictly, this may not be a correct construction, since the thermodynamic driving forces for the transformation may change discontinuously at the $(\alpha_2 + \beta_0 + O)/(O + \beta_0)$ transus and it may be more appropriate to draw two distinct TTT curves associated with each of these phase fields.

At cooling rates corresponding to FCII and FCIII, the α_2 phase is the primary decomposition product, and thus, the cooling curves corresponding to these two heat treatments are shown to intersect the TTT curve for the transformation $\beta_0 \rightarrow \alpha_2 + \beta_0$. This TTT curve must be asymptotic to the $(\alpha_2 + \beta_0)/\beta_0$ transus at 1383 K as well as the $(\alpha_2 + \beta_0 + O)/(O + \beta_0)$ transus at 1123 K. The clause of the previous paragraph regarding the continuity of the TTT curves applies to this transformation as well in passing through the $(\alpha_2 + \beta_0)/(\alpha_2 + \beta_0 + O)$ transus.

If the α_2 phase forms as the primary decomposition product, as in FCII and FCIII, then a variety of secondary reactions are possible on cooling from the $\alpha_2 + \beta_0$ phase field into the $\alpha_2 + \beta_0 + O$ phase field. The fine multivariant plate O product observed at the periphery of the α_2 plates is deduced to have precipitated from the α_2 phase based on an analysis of its orientation relationships, as in Reference 4, and thus forms by the reaction $\alpha_2 \rightarrow \alpha_2 + O$. The TTT curve for this reaction is shown to intersect the FCII cooling curve at 1253 K, since this transformation product is observed on cooling to 1253 K and then water quenching (Figure 9(b)). On cooling at the same rate to a lower temperature, 1173 K (Figure 9(c)), and also in the FCII sample (Figure 11), a monolithic rim of O phase is seen to form around the α_2 laths at the α_2/β_0 interface. The morphology of this product suggests that it has formed by a peritectoid reaction $\alpha_2 + \beta_0 \rightarrow O$, and the TTT curve for this reaction is also shown in Figure 22. Both this and the TTT curve for the reaction $\alpha_2 \rightarrow \alpha_2 + O$ are indicated as dotted lines, since these reactions are contingent on α_2 phase formation.

A variety of reactions can occur on cooling through a three-phase region of a ternary phase diagram. These include the eutectoid reaction $\beta_0 \rightarrow O + \alpha_2$, the peritectoid reactions $\beta_0 + O \rightarrow \alpha_2$ or $\beta_0 + \alpha_2 \rightarrow O$, and the reactions $\beta_0 \rightarrow \beta_0 + O$, $\beta_0 \rightarrow \beta_0 + \alpha_2$ or $\alpha_2 \rightarrow \alpha_2 + O$. Which of these occur depends on the alloy composition and the relative positions of the three-phase isotherms at different temperatures. We note, in passing, that Hillert[26] has provided a criterion to determine which reaction will occur on cooling through a given temperature decrement (see Prince[27] for an example) but that this criterion may only be applied if the three-phase isotherms at different temperatures are known.

C. *Aging Transformations*

The microstructure of samples quenched from the β phase field and subsequently aged in the $\alpha_2 + \beta_0 + O$ or $\beta_0 + O$ phase fields is quite distinct from that obtained by cooling at slower rates from the β phase field. In the latter case, α_2 or O phase precipitates in the form of Widmanstätten laths in a β_0 matrix (Figures 9 and 10), leaving behind thin films of retained β_0. This microstructure is conventionally observed in titanium alloys on β heat treatment. Aging the quenched structures,

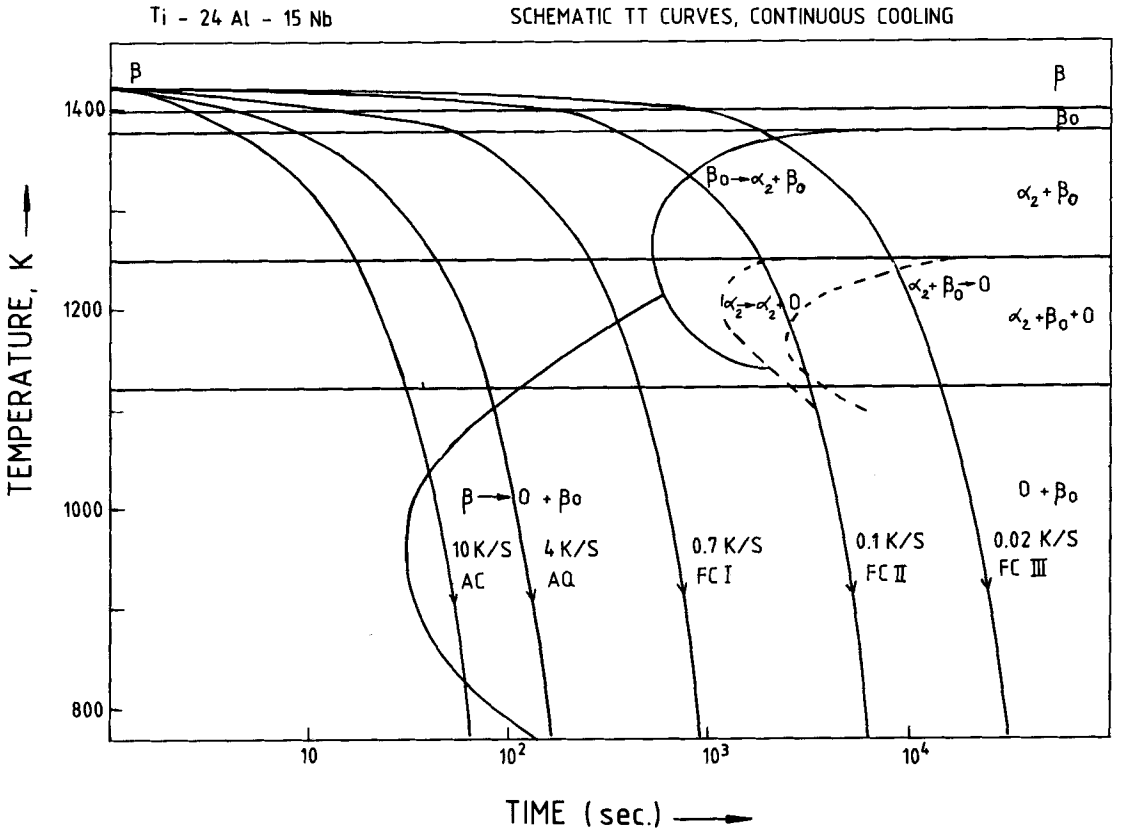

Fig. 22—Schematic TTT curves proposed for continuous cooling from the β phase field. The cooling curves employed in this study are indicated.

however, results in a microstructural appearance which suggests that α_2 and β_0 have precipitated in O (Figure 17). We have therefore carefully followed the decomposition sequence in the quenched and aged structures and report our observations in Part II.[21]

Samples aged after subtransus solution treatment show changes both in primary α_2 as well as the quenched in metastable β_0. The metastable β_0 phase after the solution treatment at 1293 K has the composition Ti-24Al-18Nb. Such a composition lies in the two-phase, O + β_0, region at temperatures at and below 1173 K (Figure 21). Thus, aging at temperatures from 1023 to 1123 K results in the decomposition of this β_0 phase to O + β_0 mixtures. The transformation proceeds through two different kinetically competitive modes which occur simultaneously at all aging temperatures—one, a conventional continuous precipitation of O in β_0 and the other resulting in β_0 precipitates within O grains. The latter microstructure is similar to that obtained by aging β WQ samples at 1073 K and is described in detail in Part II.[21]

In reporting the O phase,[4] we speculated that this phase is a derivative of α_2 and forms as a consequence of a phase separation reaction within α_2 into Nb-lean and Nb-rich regions with subsequent transformation of the Nb-rich regions to the O structure (see the free energy composition curves of Figure 15 in Reference 4). Evidence of extremely fine scale decomposition has indeed been observed within α_2 (Figures 4 and 13). It was hoped that by low-temperature aging in the two-phase O + β_0 region, as in the heat treatments MA + 1073 K and MA + 923 K (Table III), the mottled α_2 phase could be induced to decompose to O and the steps in this transformation could be observed. While a strong intensification of the tweedlike contrast within α_2 was indeed seen (Figure 15), no clear evidence that this tweed was associated with a phase separation reaction could be obtained. The tweed caused very diffuse streaking in ⟨1010⟩ directions, rather than satellite formation which normally accompanies a spinodal reaction. The nature of α_2 decomposition to O remains an area for further investigation.

V. CONCLUSIONS

1. The phase fields β, β_0, $\alpha_2 + \beta_0$, $\alpha_2 + \beta_0$ + O, and β_0 + O have been identified in a Ti-24Al-15Nb alloy, and an isothermal section showing the tie triangle for the $\alpha_2 + \beta_0$ + O phase field at 1173 K has been developed.
2. The chemistry of the α_2 and β_0 phases of the Ti-24Al-15Nb alloy has been determined as a function of temperature in the two-phase $\alpha_2 + \beta_0$ field and compared with earlier data on the Ti-24Al-11Nb alloy. Increasing the Nb concentration at the constant Al level of 24 at. pct results in an increase of Al and Nb levels in both the α_2 and β_0 phase. The O phase in the three-phase region of $\alpha_2 + \beta_0$ + O has an Al level identical to that of the α_2 phase but is enriched in Nb; that is, tie lines in the two-phase α_2 + O region at 1173 K are likely to run parallel to constant Al lines.
3. The sequence of phase fields in this alloy results in complex microstructures for samples cooled at

different rates from above the β transus. The kinetics of β transformation to α_2 or O are such that faster cooling rates result in β transformation directly to O phase rather than to α_2, even though the samples pass through $\alpha_2 + \beta_0$ and $\alpha_2 + \beta_0 + O$ phase fields in the cooling process. In samples cooled more slowly, on the other hand, the β phase transforms first to the α_2 phase, which subsequently decomposes partially to O, or transforms to O through the reaction $\beta_0 + \alpha_2 \rightarrow O$.

4. The aging transformations for both β water-quenched and subtransus solution-treated samples proceed through β decomposition modes, which result in microstructures quite distinct from those arising from conventional continuous precipitation of α_2/O in β_0. The nature of these alternative decomposition modes is studied in greater detail in Part II.[21]

ACKNOWLEDGMENTS

This work was funded by the Defence Research and Development Organisation, India. The encouragement of the Director, DMRL, and his kind permission to publish these results are acknowledged. The authors also wish to thank Professor K.S. Raghavan of the Department of Metallurgy, Indian Institute of Technology, Madras, for allowing one of us (K. Muraleedharan) to use his analytical electron microscopy facilities.

REFERENCES

1. M.J. Blackburn, D.L. Ruckle, and C.E. Bevan: U.S. Air Force Technical Report, AFML-TR-78-18, 1978.
2. M.J. Blackburn and M.P. Smith: U.S. Air Force Technical Report, AFML-TR-80-4175, 1980.
3. M.J. Blackburn and M.P. Smith: U.S. Air Force Technical Report, AFML-TR-82-4086, 1982.
4. D. Banerjee, A.K. Gogia, T.K. Nandy, and V.A. Joshi: *Acta Metall.*, 1988, vol. 36, pp. 871-82.
5. L.A. Bendersky, W.J. Boettinger, B.P. Burton, F.S. Biancaniello, and C.B. Shoemaker: *Acta Metall.*, 1990, vol. 38, pp. 931-43.
6. R. Strychor, J.C. Williams, and W.A. Soffa: *Metall. Trans. A*, 1988, vol. 19A, pp. 225-34.
7. L.A. Bendersky and W.J. Boettinger: *High Temperature Ordered Intermetallic Alloys III*, C.T. Liu, A.I. Taub, N.S. Stoloff, and C.C. Koch, eds., MRS, Pittsburgh, PA, 1989, pp. 45-50.
8. J.H. Perepezko, Y.A. Chang, L.E. Seitzman, J.C. Lin, N.R. Bonda, T.J. Jewett, and J.C. Mishurada: *High Temperature Aluminides and Intermetallics*, S.H. Whang, C.T. Liu, D.P. Pope, and J.O. Stiegler, eds., TMS/ASM INTERNATIONAL, Warrendale, PA, 1990, pp. 19-47.
9. T.J. Jewett, J.C. Lin, K.C. Hsieh, N.R. Bonda, Y.A. Chyang, and J.H. Perepezko: *High Temperature Ordered Intermetallic Alloys III*, C.T. Liu, A.I. Taub, N.S. Stoloff, and C.C. Koch, eds., MRS, Pittsburgh, PA, 1989, pp. 69-74.
10. D. Banerjee, T.K. Nandy, A.K. Gogia, and K. Muraleedharan: *6th World Conf. on Titanium*, P. Lacombe, R. Tricot, and G. Beranger, eds., *J. Phys.*, Les Ulis, France, 1989, pp. 1091-96.
11. M.J. Kaufman, J.F. Broderick, C.H. Ward, R.G. Rowe, and F.H. Froes: *6th World Conf. on Titanium*, P. Lacombe, R. Tricot, and G. Beranger, eds., *J. Phys.*, Les Ulis, France, 1989, pp. 985-90.
12. H.T. Kestner-Weykamp, C.H. Ward, T.F. Broderick, and M.J. Kaufman: *Scripta Metall.*, 1989, vol. 23, pp. 1697-1702.
13. H.T. Kestner-Weykamp, D.R. Baker, D.M. Paxton, and M.J. Kaufman: *Scripta Metall.*, 1990, vol. 24, pp. 445-50.
14. R.G. Rowe: *High Temperature Aluminides and Intermetallics*, S.H. Whang, C.T. Liu, D.P. Pope, and J.O. Stiegler, eds., TMS/ASM INTERNATIONAL, Warrendale, PA, 1990, pp. 375-401.
15. A.K. Gogia, D. Banerjee, and T.K. Nandy: *Metall. Trans. A*, 1990, vol. 21A, pp. 609-25.
16. J.M. Larsen, K.A. Williams, S.J. Balsone, and M.A. Stucke: *High Temperature Aluminides and Intermetallics*, S.H. Whang, C.T. Liu, D.P. Pope, and J.O. Stiegler, eds., TMS/ASM INTERNATIONAL, Warrendale, PA, 1990, pp. 521-56.
17. R.A. Spurling: *Metall. Trans. A*, 1975, vol. 6A, pp. 1660-61.
18. K. Muraleedharan and D. Banerjee: *Metall. Trans. A*, 1989, vol. 20A, pp. 1139-42.
19. K. Muraleedharan, S.V. Nagender Naidu, and D. Banerjee: *Scripta Metall.*, 1990, vol. 24, pp. 27-32.
20. A.K. Gogia: Ph.D. Thesis, Defence Metallurgical Research Laboratory, Hyderabad, India, and Banaras Hindu University, Varanasi, India, 1990.
21. K. Muraleedharan, T.K. Nandy, and D. Banerjee: *Metall. Trans. A*, 1992, vol. 23A, pp. 417-31.
22. F.N. Rhines: *Phase Diagrams in Metallurgy*, McGraw Hill, New York, NY, 1956, p. 85.
23. J.L. Murray: *Binary Alloy Phase Diagrams*, T.B. Massalski, ed., ASM, Metals Park, OH, 1986, pp. 173-76.
24. W.A. Baeslack III and T. Broderick: *Scripta Metall.*, 1990, vol. 24, pp. 319-24.
25. J.A. Peters and C. Bassi: *Scripta Metall.*, 1990, vol. 24, pp. 915-20.
26. M. Hillert: *J. Iron Steel Inst.*, 1958, vol. 189, p. 224.
27. A. Prince: *Alloy Phase Equilibria*, Elsevier, London, 1966, pp. 152-59.
28. A.K. Gogia, D. Mukherjee, and D. Banerjee: Defence Metallurgical Research Laboratory, Hyderabad, India, unpublished research, 1990.